Supporting Information for

The effect of amorphization on the molecular motion of the 2-methylimidazolate linkers in ZIF-8

Naoki Ogiwara,[a] Daniil I. Kolokolov,*[b,c] Masaki Donoshita,[a] Hirokazu Kobayashi,[a,d] Satoshi Horike[e] Alexander G. Stepanov,[b,c] and Hiroshi Kitagawa*[a,e]

[a] Division of Chemistry, Graduate School of Science, Kyoto University, Kitashirakawa-Oiwakecho, Sakyo-ku, Kyoto 606-8502, Japan

[b] Boreskov Institute of Catalysis, Siberian Branch of Russian Academy of Sciences, Prospekt Akademika Lavrentieva 5, Novosibirsk 630090, Russia

[c] Department of Physical Chemistry, Faculty of Natural Sciences, Novosibirsk State University, Pirogova Street 2, Novosibirsk 630090, Russia

[d] PRESTO, Japan Science and Technology Agency, 4-1-8 Honcho, Kawaguchi, Saitama 332-0012, Japan

[e] Institute for Integrated Cell-Material Sciences, Institute for Advanced Study, Kyoto University, Yoshida-Honmachi, Sakyo-ku, Kyoto 606-8501, Japan

mailto:kdi@catalysis.ru; kitagawa@kuchem.kyoto-u.ac.jp

1. Experimental procedures

Synthesis of deuterated 2-methylimidazole (2-mIM-d_6)

Protonated 2-methylimidazole (2-mIM) was deuterated according to a modified procedure.[1] 2-mIM (6.3 g, TCI Chemicals, Japan) and PtO_2 (0.11 g, FUJIFILM Wako Pure Chemical Corporation, Japan) were added to D_2O (60 mL, FUJIFILM Wako Pure Chemical Corporation, Japan) in a 100 mL vessel. After sealing the vessel, it was heated at without stirring 250 °C for 20 h. After cooling, the obtained crystals were dissolved in MeOH (50 mL), filtered to separate the PtO_2, and evaporated to remove the D_2O and MeOH. The powder samples thus obtained were then added to D_2O (60 mL) with PtO_2 (0.11 g) in a 100 mL vessel and heated at 250 °C for 20 h. After cooling, the obtained crystals were, once again, dissolved in MeOH (50 mL), filtered to separate the PtO_2, and evaporated to remove the D_2O and MeOH. The powder samples thus obtained were purified by sublimation. The D/H ratio was > 98%, as characterized by ^{1}H NMR.

Synthesis of ZIF-8

Perdeuterated ZIF-8 material was synthesized according to a modified procedure.[2] A solution of $Zn(NO_3)_2 \cdot 6H_2O$ (0.8 g, FUJIFILM Wako Pure Chemical Corporation) in MeOH (25 mL) was rapidly poured into a solution of 2-mIM-d_6 (1.7 g) in MeOH (25 mL) while stirring at room temperature (pH of the solution was mediated by NaOH). After 1 h of stirring, the product that formed was separated from the mother solution by centrifugation. The resulting white crystals were washed with deionized H_2O (3 × 50 mL) and MeOH (3 × 50 mL). The product was then dried at 150 °C for 15 h under vacuum.

Synthesis of amorphous ZIF-8 (a_mZIF-8)

a_mZIF-8 was prepared by a ball milling method as previously reported.[3] A 10 mL stainless steel jar was charged with 100 mg of the ZIF-8 crystals and a 10 mm stainless steel milling ball at room temperature and then well sealed. This combination was subjected to 30 Hz milling in a Retsch MM400 grinder mill for 30 min.

Characterizations

Powder X-ray diffraction (PXRD) measurements were recorded on a Rigaku Miniflex 600 diffractometer with Cu $K\alpha$ radiation. The scan step was 0.02°. N_2 sorption isotherms were

collected at 77.4 K using volumetric techniques (BELSORP-Max, Microtrac BEL Corp., Japan). All samples were activated over 15 h at 423 K under vacuum. Zn *K*-edge X-ray absorption spectra (XAS) were collected on the BL14B2 beamline at SPring-8 in transmission mode under ambient conditions, using a Si (311) double crystal monochromator. The data were processed with IFEFFIT.[4] Fourier transformation was k^3-weighted in the k range from 2.5 to 15.6 $Å^{-1}$.

Sample preparation for NMR measurements

Samples for NMR measurements were prepared as follows. About 0.1 g of powder sample was loaded into a 5 mm glass tube, connected to a vacuum line, then heated at 423 K for 15 h under vacuum to a final pressure above the sample of 10^{-2} Pa. The neck of the tube was then sealed off, while the material sample was held in liquid nitrogen in order to prevent it from being heated by the flame. The sealed sample was then transferred into an NMR probe for analysis by ^{2}H NMR spectroscopy.

^{2}H NMR measurements

^{2}H NMR experiments were performed at Larmor frequency $\omega_z/(2\pi)$ = 61.42 MHz on a Bruker Avance II$^+$ 400 MHz NMR spectrometer (Bruker Biospin K.K.) using a high-power probe with a 5 mm horizontal solenoid coil. In addition to the wide temperature range high power (HP) probe, a low temperature (LT) HP probe was used to conduct NMR measurements at temperatures below 100 K. All ^{2}H NMR spectra were obtained by Fourier transformation of quadrature-detected phase-cycled quadrupole echo arising in the pulse sequence ($90°_x - \tau_1 - 90°_y - \tau_2 -$ acquisition $- t$), where τ_1 = 20 μs, τ_2 = 21 μs, and t is a repetition time of the sequence during the accumulation of the NMR signal. The duration of the $\pi/2$ pulse was 1.7–2.0 μs. Spectra were typically acquired with 12–64 scans, with repetition time ranging from 1–250 s. Inversion–recovery experiments to derive spin–lattice relaxation times (T_1) were carried out using the pulse sequence ($180°_x - \tau_v - 90°_{\pm x} -$ acquisition $- t$), where t_v is a variable delay between the 180° and 90° pulses. The temperature of the samples was controlled with a flow of N_2 or He gas by a variable temperature unit BVT-3000, with a precision of about 1 K.

^{2}H NMR T_1 and T_2 relaxation simulation

To understand the detailed mechanism of rotations and their kinetic parameters (the activation barriers and rate constants), a detailed fitting analysis of the ^{2}H NMR spin relaxation within the experimentally studied temperature range was performed. Our "homemade" FORTRAN simulation routines were based on the general formalism proposed by Abragam[5] and developed in detail by Spiess[6] and others.[7-10]

Spin relaxation times T_1 and T_2 are generally anisotropic and depend on the observation angles θ and φ in the powder pattern. They are given by the usual formulae[6]

$$\frac{1}{T_1} = \frac{3}{4}\pi^2 \, Q_0^2 \, (J_1(\omega_0) + 4J_2(2\omega_0)) \tag{1}$$

$$\frac{1}{T_2} = \frac{3}{8}\pi^2 \, Q_0^2 \, (3J_0(0) + 5J_1(\omega_0) + 2J_2(2\omega_0)) \tag{2}$$

where $Q_0 = \frac{e^2 q Q_{2H}}{h}$ is the quadrupolar coupling constant for the ^{2}H nuclei in Hz. The spectral density function $J_m(\omega)$ for the chosen model of the molecular motion is defined by the expression

$$J_m(\omega) = 2 \sum_{a,b=-2}^{2} D_{a,q}(\Omega_L)^* \, D_{b,q}(\Omega_L) \otimes G_{0,a|0,b}(\omega) \tag{3}$$

where

$$G_{c,a|d,b}(\omega) = \sum_{l,k,n=1}^{N} D^{\,l}_{c,a}(\Omega_l)^* \, D^{\,k}_{d,b}(\Omega_k) p_{eq}(l) V_{l,n} \left(\frac{-\lambda_n}{{\lambda_n}^2 + \omega^2} \right) V^{-1}_{n,k} \tag{4}$$

Here, Ω_L represents the observation angles θ and φ, which connect the molecular frame with the laboratory frame, and Ω_k represents the Euler angles, which connect the molecular frame with the k-th distinct position of the *C–D* bond within the assumed geometry of the jump model; $V_{l,n}$ is a matrix comprising Eigen vectors of the kinetic matrix K and λ_n represents the Eigen values; N is the number of distinct jump sites.

If one or multiple isotropic motions are present, then the corresponding correlation function is no longer dependent on the polar angles and the resulting function is simply a tensor multiplication of correlation functions for distinct motional modes. In the present case, we used a complex model

where the spectral function is a tensor multiplication of two, assumed to be independent, spectral functions.

$$J_m(\omega) = 2 \sum_{\substack{a,b=-2 \\ c,d}}^{2} D_{a,q}(\Omega_L)^{*} D_{b,q}(\Omega_L) \otimes G^1{}_{c,a|d,b}(\omega) \otimes G^2{}_{0,c|0,d}(\omega) \quad (5)$$

Here G^1 takes into account the fast anisotropic librations, while G^2 defines the slow librations and the slow large amplitude twist. In both cases, the functions are computed using equation 4. The libration models are constructed by a free exchange with rate $k_{\mathrm{lib}}{}^{\mathrm{i}}$ between n^{i} equally populated sites. Each site represents one of the possible orientations (given by the axial rotation angle, φ) of the linker plane located within the limiting sector $\pm\Delta\varphi^{\mathrm{i}}$. The large amplitude twist is defined as a two-site exchange between the equilibrium positions with $\varphi_1 = 0$ and $\varphi_2 = \varphi^{\mathrm{c}}$. In the latter case, in addition to the rate and geometrical parameters, the equilibrium population of the second site is also a variable parameter.

2. PXRD measurements of a_{m}ZIF-8

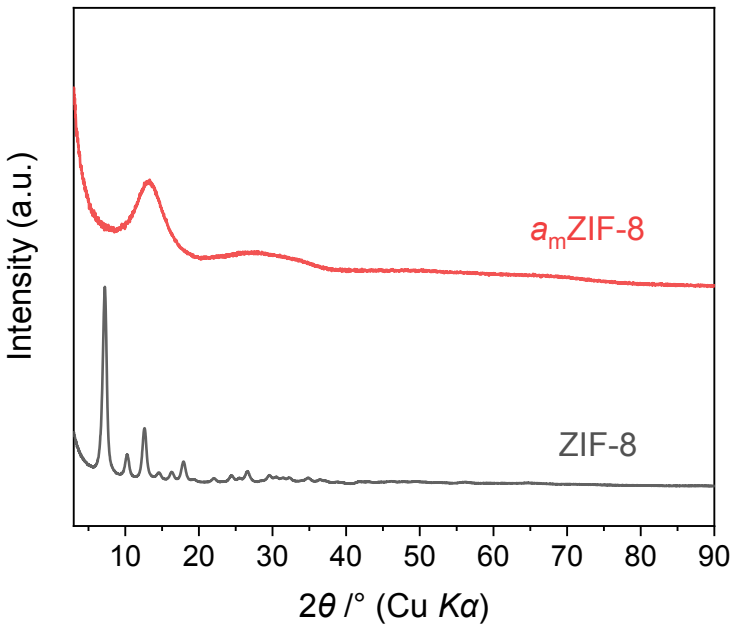

Figure S1. PXRD patterns of ZIF-8 (black) and a_{m}ZIF-8 (red).

3. XAS of a_mZIF-8

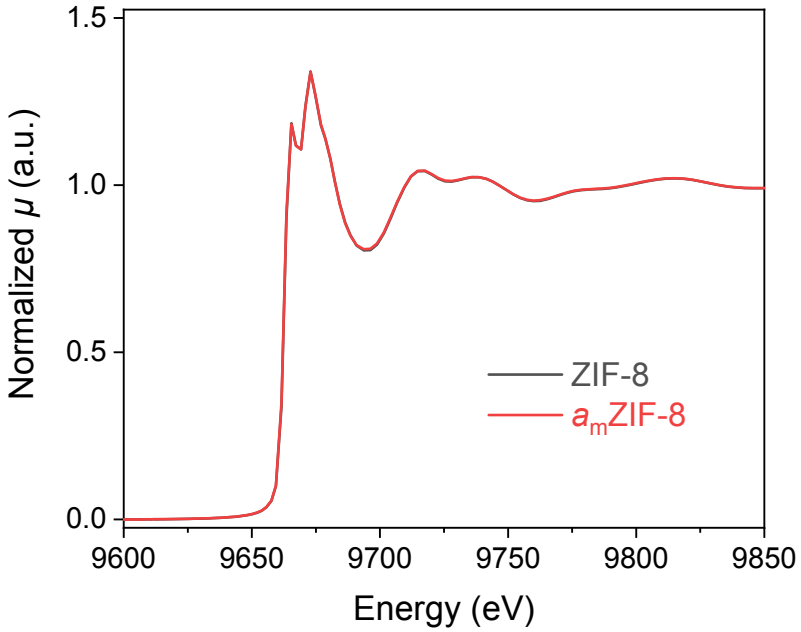

Figure S2. Zn-*K* edge X-ray absorption near-edge structure spectra of ZIF-8 (black) and a_mZIF-8 (red).

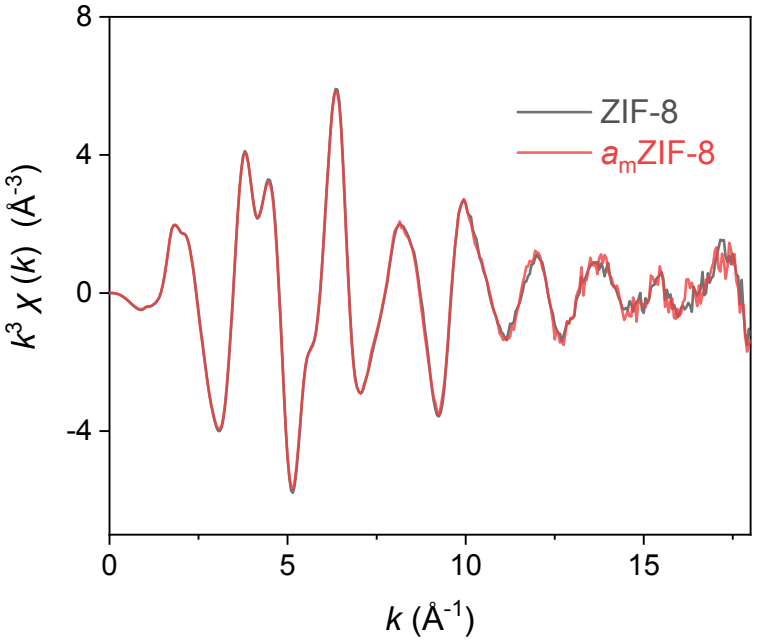

Figure S3. Zn-*K* edge extended X-ray absorption fine-structure spectra of ZIF-8 (black) and a_mZIF-8 (red).

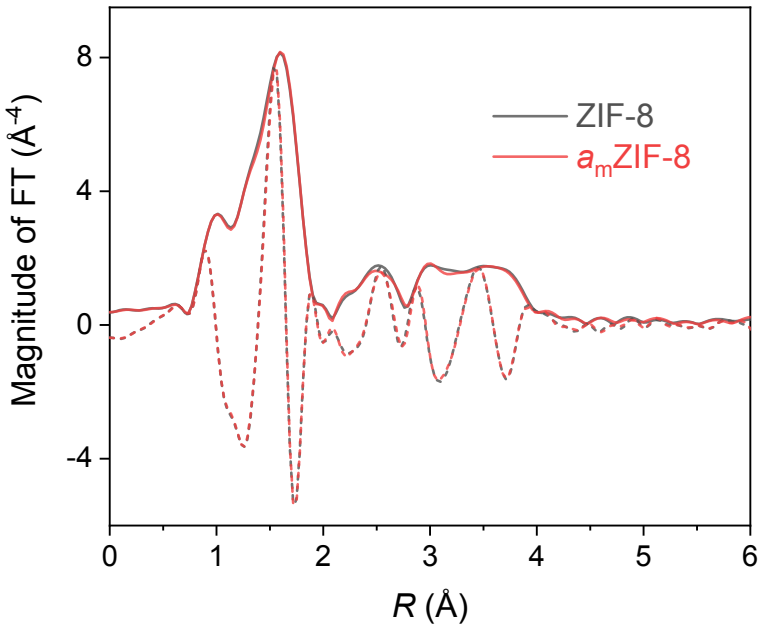

Figure S4. Fourier transform (FT) of the X-ray absorption fine-structure spectra of ZIF-8 (black) and a_mZIF-8 (red).

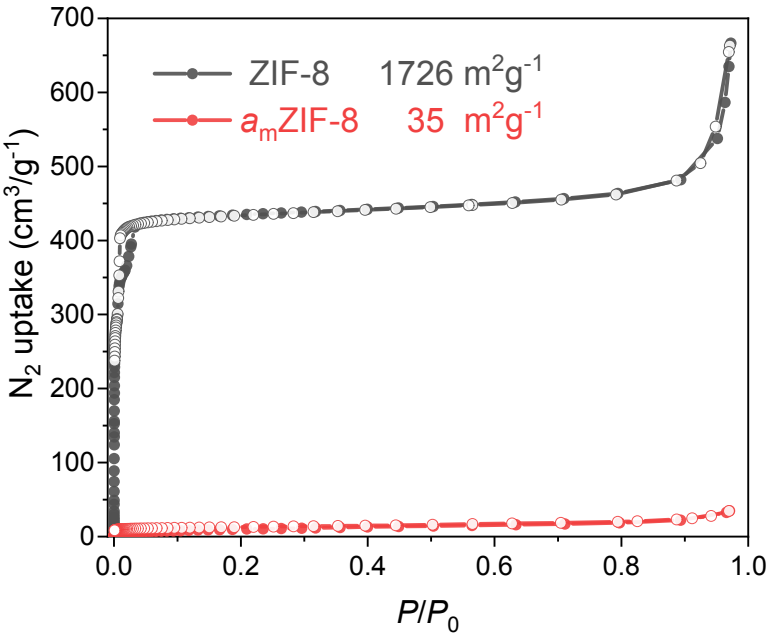

Figure S5. N_2 sorption isotherms of ZIF-8 (black) and a_mZIF-8 (red). Closed circles indicate adsorption and open circles indicate desorption.

4. ^{2}H NMR relaxation of a_m-ZIF-8

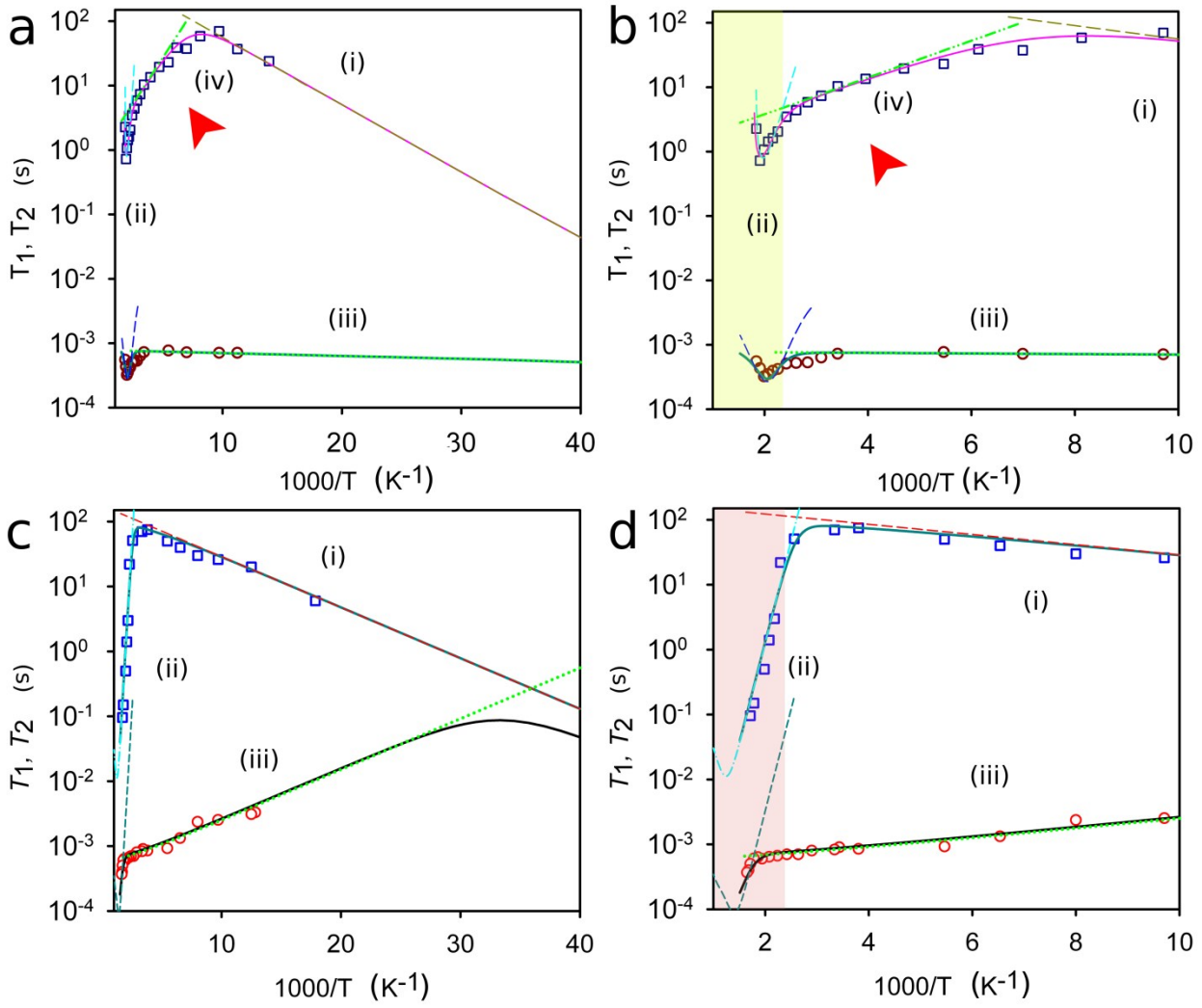

Figure S6. ^{2}H NMR T_1 (squares) and T_2 (circles) relaxation curves as a function of temperature for the CD group of the deuterated 2-mIM linker in: (a) amorphous ZIF-8, (b) amorphous ZIF-8, (c) crystalline ZIF-8, and (d) crystalline ZIF-8 on a narrowed temperature scale. The numerical simulation results are given by solid lines, while the dashed lines emphasize individual motional modes.

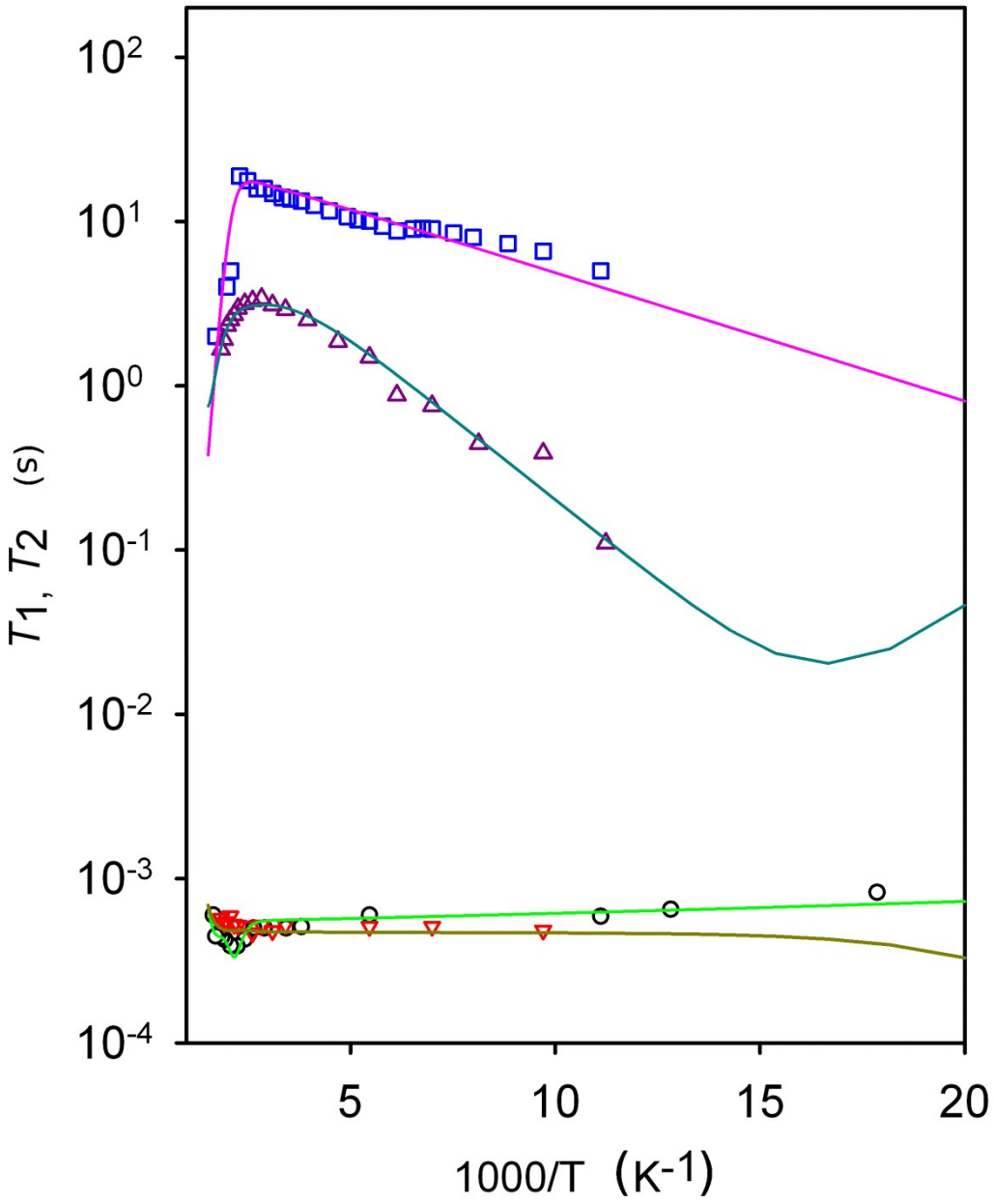

Figure S7. ^{2}H NMR T_1 and T_2 relaxation curves as a function of temperature for the CD_3 group of the deuterated 2-mIM linker in: T_1 (Δ) amorphous ZIF-8, T_2 (∇) amorphous ZIF-8, T_1 (□) crystalline ZIF-8, and T_2 (○) crystalline ZIF-8. The numerical simulation results are given by solid lines.

References

1. M. Yamamoto, Y. Yokota, K. Oshima and S. Matsubara, *Chem. Commun.*, 2004, 1714.

2. D. I. Kolokolov, A. G. Stepanov and H. Jobic, *J. Phys. Chem. C*, 2015, **119**, 27512.

3. T. D. Bennett, S. Cao, J. C. Tan, D. A. Keen, E. G. Bithell, P. J. Beldon, T. Friščić and A. K. Cheetham, *J. Am. Chem. Soc.*, 2011, **133**, 14546.

4. B. Ravel and M. Newville, *J. Synchrotron Radiat.*, 2005, **12**, 537–541.

5. A. Abragam, *The Principles of Nuclear Magnetism*, Oxford University Press, Oxford, UK, 1961.

6. H. W. Spiess, in *NMR: Basic Principles and Progress*, ed. P. Diehl, E. Fluck and R. Kosfeld, Springer-Verlag, New York, 1978, vol. 15, p 55–214.

7. R. J. Wittebort and A. Szabo, *J. Chem. Phys.*, **1978**, *69*, 1722.

8. R. J. Wittebort, E. T. Olejniczak and R. G. Griffin, *J. Chem. Phys.*, **1987**, *86*, 5411.

9. G. Lipari and A. Szabo, *Biophys. J.*, **1980**, *30*, 489.

10. L. J. Schwartz, E. Meirovitch, J. A. Ripmeester and J. H. Freed, *J. Phys. Chem.*, **1983**, *87*, 4453.